Space-filling properties of polydisperse granular media

C. Voivret,* F. Radjaï, J.-Y. Delenne, and M. S. El Youssoufi
LMGC, CNRS-Université Montpellier II, Place Eugène Bataillon, 34095 Montpellier cedex, France
(Received 21 May 2007; revised manuscript received 3 July 2007; published 2 August 2007)

We present a systematic investigation of the morphology and space-filling properties of polydisperse densely packed granular media in two dimensions. A numerical procedure is introduced to generate collections of circular particles with size distributions of variable shape and span constrained by explicit criteria of statistical representativity. We characterize the domain of statistically accessible distribution parameters for a bounded number of particles. This particle generation procedure is used with two different deposition protocols in order to build large close-packed samples of prescribed polydispersity. We find that the solid fraction is a strongly nonlinear function of the size span, and the highest levels of solid fraction occur for the uniform distribution by volume fractions. As the span is increased, a transition occurs from a regime of topological disorder where the packing properties are governed by particle connectivity to a regime of metric disorder where pore-filling small particles prevail. The polydispersity manifests itself in the first regime through the variability of local coordination numbers. We observe a continuous decrease of the number of particles with four contacts and the growth of two populations of particles with three and five contacts. In the second regime, radial distribution functions show that the material is homogeneous beyond only a few average particle diameters. We also show that the packing orientational order is linked with fabric anisotropy and it declines with size span.

DOI: 10.1103/PhysRevE.76.021301 PACS number(s): 45.70.−n, 81.05.Rm, 61.43.Hv

I. INTRODUCTION

Size polydispersity is a generic feature of granular materials. Most soils, powders, and natural composites involve a broad range of particle sizes produced by fragmentation and aggregation processes [1,2]. In industry, size polydispersity appears as a major factor that needs to be optimized for high-peformance applications. A well-known example is concrete in which broad size distribution leads to reduced porosity and thus enhanced strength [3–5]. On the other hand, the pore space characteristics, which are important in chemical engineering for liquid flow (e.g., water retention) and the adsorbent action of particles (e.g., filtering), depend directly on the particle size distribution [6–9].

Among many aspects of essentially geometrical nature concerned with polydisperse packings, at least two issues are of fundamental interest: (1) space-filling properties, and (2) packing structure in terms of connectivity and structural order. The space-filling issue corresponds mainly to the highly polydisperse regime where numerous particles of sufficiently small size can fill the pore space between larger particles [10,11]. On the other hand, the question of packing structure is often associated with the weakly polydisperse regime where structural order is drastically altered due to a weak polydispersity. This is the case in two dimensions (2D) where long-range order in a monodisperse packing disappears due to a narrow size distribution [12,13].

Particle size distribution $N(d)$ is a major characteristic of geomaterials, and polydisperse granular materials have been extensively investigated in soil mechanics [14]. The size distribution is often represented by the cumulate volume distribution (CVD) of the particles, often referred to as a grading curve in soil mechanics. Different descriptors of particle size distribution, such as the coefficients of uniformity and curvature, are used to characterize the soils [14]. Few studies about the impact of these descriptors on the mechanical behavior show that the shear strength increases with solid fraction [15].

The investigation of microstructure for strongly polydisperse materials has been hampered by measurement difficulties. Analytical studies of packings constructed according to various space-filling strategies also exist mainly for the case of power-law size distribution and apollonian or random apollonian constructions [10,11,16]. More general packing properties can be more easily reached by means of numerical simulations. Nevertheless, dynamic simulation methods such as contact dynamics and molecular dynamics, are deficient in the number of tractable particles. Indeed, a broad size distribution with well-represented classes of different sizes requires many more particles than a narrow size distribution often used in numerical simulations of granular media [17,18].

In this paper, we introduce a numerical procedure to generate collections of circular particles with a prescribed CVD and explicit criteria of statistical representativity. Although this procedure is quite general, we will use the β function to represent CVDs. This function involves three parameters, and depending on the position in the parameter space, the resulting CVD can be simple- or double-curved. Moreover, particular size distributions such as monodisperse, bidisperse, uniform in diameter, or of power-law shape can be generated. We will show that statistically well-represented distributions can be obtained only for a portion of the parameter space when the total number of data (particle diameters) cannot exceed an upper bound for practical reasons such as numerical tractability. This is the case whenever the distribution involves numerous small particles.

This size generation procedure is then used within a ballistic deposition algorithm in order to build very large close-packed samples of desired polydispersity [19]. Deposition algorithms are based on purely geometrical rules and they have been applied to investigate surface growth and packing

*voivret@lmgc.univ-montp2.fr

structure or to construct dense packings as input to dynamics simulations [20–24]. However, only monodisperse or weakly polydisperse packings have been considered in the past.

The close-packed samples produced by the generation procedure together with a deposition protocol allow us to investigate various descriptors of granular microstructure as a function of polydispersity parameters. Two issues will be addressed in more detail: (1) How particle size distribution (width, shape) affects the space-filling properties in terms of solid fraction; and (2) How deviation from the monodisperse limit affects structural order (translational and angular) in terms of radial distribution function and contact network anisotropy.

In the following, we introduce in Sec. II our numerical procedures with focus on the size generation method. In Sec. III we study the parametric space, statistically accessible domains, finite-size effects, and the coefficient of uniformity. Then, in Secs. IV and V we present our main findings concerned with space-filling and morphological properties of the granular microstructure. We will conclude with a summary and perspectives of this work.

II. NUMERICAL PROCEDURES

A. Particle generation

We assume that the CVD of the particles is represented by a continuous function $h(d)$ of particle diameters d varying in the range $[d_{\min}, d_{\max}]$. By definition, we have

$$h(d) = \frac{\int_{d_{\min}}^{d} V(x)N(x)dx}{\int_{d_{\min}}^{d_{\max}} V(x)N(x)dx}, \tag{1}$$

where $N(d)$ is the particle size distribution and $V(x) = (\pi/4)x^2$ is the 2D volume of a particle of diameter d. We have $h(d_{\min})=0$ and $h(d_{\max})=1$. Since the CVD represents volume cumulate of the particles, we first discuss here how the corresponding cumulative distribution function $F(d)$ of particle diameters can be obtained.

The CVD defined over the interval $[d_{\min}, d_{\max}]$ is first discretized into N_c "classes" defined over subintervals $[d^i_{\min}, d^i_{\max}]$ of widths $\Delta d_i \equiv d^i_{\max} - d^i_{\min}$ and $i \in [1, N_c]$. Then, the CVD is decumulated over each interval in order to obtain the volume fraction f^i_v for each class i as follows:

$$f^i_v = h(d^i_{\max}) - h(d^i_{\min}). \tag{2}$$

We require that the following two "representativity" conditions be satisfied: (1) The number of particles in each class is above a minimum $N'_{p/c}{}^{,\min}$. (2) The volume of each particle in a class i is small compared to the total volume f^v_i of the class. We note that these two conditions are equivalent for a quasi-monodisperse distribution.

We further assume that the CVD is linear over each class i. This condition implies that the cumulative distribution function $F^i(d)$ of particle diameters over the class i is a normalized uniform distribution by volume fractions of particles defined over the interval $[d^i_{\min}, d^i_{\max}]$ as follows:

$$F^i(d) = \frac{d^i_{\max}}{d^i_{\max} - d^i_{\min}} \frac{d - d^i_{\min}}{d}. \tag{3}$$

Then, the mean diameter $d^i_m = (F^i)^{-1}(0.5)$ of the class can be estimated. This information allows us to determine the amount n^i of the particles in the class for a unit total volume as follows:

$$n^i = \frac{4f^v_i}{\pi (d^i_m)^2}. \tag{4}$$

Each n^i is then rescaled by a factor $N'_{p/c}{}^{\min}/\min\{n^i\}$ and its integer part corresponds to the temporary number of particles N'^i in the class i as follows:

$$N'_i = \text{int}\left\{ \frac{N'_{p/c}{}^{\min}}{\min\{n^i\}} n^i \right\}, \tag{5}$$

where int is the integer part. This procedure ensures that each class will contain at least $N'_{p/c}{}^{\min}$ particles as required by the first representativity condition.

The total number of particles $N'_p = \Sigma_i N'^i$ obtained at this stage is dependent on the parameters N_c and $N'_{p/c}{}^{\min}$. But, N'_p may be deficient for the construction of a representative packing. Let $N^{\min}_p$ be the minimum number of particles required for the construction of the packing. We impose that the number N_p of particles should be above $N^{\min}_p$. If $N'_p < N^{\min}_p$, we rescale the N'_i by $N^{\min}_p/N'_p$ to get the number of particles N^i in each class i as follows:

$$N^i = \text{int}\left\{ \frac{N^{\min}_p}{N'_p} N'^i \right\}. \tag{6}$$

From the number of particles N^i in each class i, the probability distribution function $P^i(d)$ of particle diameters d for each class i is given by

$$P^i(d) = \frac{N^i}{N_p}, \tag{7}$$

and the cumulative distribution function $F(d)$ is obtained by summing up the P^i over all diameters $\leq d$. Given the population N^i in each class i, we generate the N^i diameters d in the class by inverse transform sampling of $F^i(d)$ given by Eq. (3).

B. Cumulate volume distribution

For our parametric study, we need a model for the CVD. Obviously, the procedure detailed above can be applied to generate statistical ensembles of particle diameters from any given CVD. However, for a parametric study the distribution parameters should be identified and varied systematically.

For practical reasons, this model of CVD should (1) be simple, i.e., involving a small number of parameters, (2) be capable of representing double-curved distributions as observed in geomaterials, (3) contain particular distributions such as power laws, and (4) be defined over a finite interval. A distribution that satisfies these requirements is the cumulative β distribution defined as

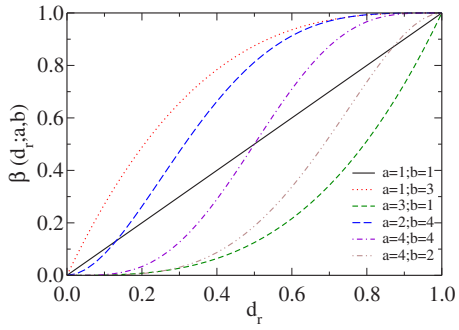

FIG. 1. (Color online) Cumulate volume distribution as a function of the relative diameter d_r for several values of the distribution shape parameters a and b according to Eq. (11).

$$\beta(x) = \frac{1}{B(a,b)} \int_0^x t^{a-1}(1-t)^{b-1} dt, \tag{8}$$

where $a>0$ and $b>0$ are the parameters of the distribution and

$$B(a,b) = \Gamma(a)\Gamma(b)/\Gamma(a+b), \tag{9}$$

where Γ is the Gamma function. This β distribution is defined and normalized over the interval $[0,1]$, so that $\beta(0)=0$ and $\beta(1)=1$.

For using the cumulative β distribution as a model of CVD for the particle diameters d over the interval $[d_{\min}, d_{\max}]$, we replace x by the reduced diameter d_r defined as

$$d_r(d) = \frac{d - d_{\min}}{d_{\max} - d_{\min}}. \tag{10}$$

Then, the CVD is defined by setting $x=d_r$ in Eq. (8) as follows:

$$h(d) = \beta[x = d_r(d); a, b]. \tag{11}$$

Since only the relative particle diameters are relevant for space-filling properties, we will use throughout this paper the reduced diameter d_r instead of d. In the same way, the span s of the distribution $h(d)$ in Eq. (11) will be defined as

$$s = \frac{d_{\max} - d_{\min}}{d_{\max} + d_{\min}}. \tag{12}$$

The case $s=0$ represents a monodisperse packing whereas $s=1$ corresponds to "infinite" polydispersity. In practice, the limit $d_{\min}=0$ never happens, and hence the span s is always strictly below unity.

In terms of reduced diameters d_r, the shape of the CVD is controlled by the parameters a and b. Figure 1 displays several plots of CVD as defined by Eq. (11) as a function of d_r for several values of a and b. The case $a=b=1$ corresponds to uniform distribution by volume fractions and appears as a straight line in Fig. 1. The CVD is double curved if $a>1$ and $b>1$. If $a=1$ and $b>1$, the distribution is strictly convex whereas if $a>1$ and $b=1$, it is strictly concave. These two cases ($a=1$ or $b=1$) correspond to power-law distributions. The uniform distribution by particle diameters is obtained for $a=3$ and $b=1$. On the other hand, for very large values of a and b, the distribution becomes quasimonodisperse. Finally, for $a<1$ and $b<1$, the distribution is nearly bidisperse with increasing concentrations around $d_r=0$ and $d_r=1$ as a and b decrease.

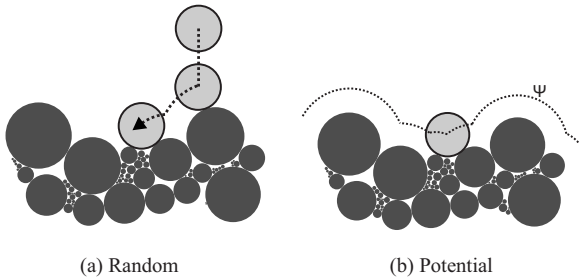

FIG. 2. Illustration of random (a) and potential-based (b) deposition methods.

C. Packing preparation

For the construction of polydisperse packings from the particle size ensembles generated according to the numerical procedure described above, we use a deposition protocol. It consists of layer-by-layer deposition of rigid particles on a substrate (a rough or smooth plane in 3D or line in 2D) according to simple geometrical rules.

Obviously, particle deposition can also be simulated by means of dynamic methods, such as molecular dynamics [25,26] and contact dynamics [27–29] in the spirit of a real experiment where the grains are poured into a box. Such simulations require, however, substantially more computation time than a purely geometrical approach.

In a deposition algorithm, the particles are allowed to "fall" sequentially over a horizontal substrate. Upon contact with the substrate or the first already deposited particle, the falling particle either sticks or is further moved geometrically to a more favorable position. This corresponds to a local relaxation rule. Alternatively, the position of the falling particle can be determined according to a global criterion such as the lowest position at the free surface or the minimum of a predefined potential energy of the particle [24]. The deposition models can be efficiently implemented in a computer code for generating very large two- and three-dimensional packings [19,30]. They have been extensively employed, rather with monodisperse particles, to investigate the growth of a granular bed or colloidal aggregates [23,31].

We use two different deposition protocols in two dimensions: (1) random and (2) potential-based. In the random model, the horizontal position of the falling particle is random. When the particle comes into contact with the first already deposited particle, it is allowed to roll until a second contact is formed with another deposited particle; see Fig. 2(a). This rule mimics the behavior of a particle placed on top of a granular bed. The particle will relax under the action of its own weight along the steepest descent to a stable position ensured by the contacts formed with the underlying particles and such that the center of mass of the deposited particle lies between the two supporting contacts.

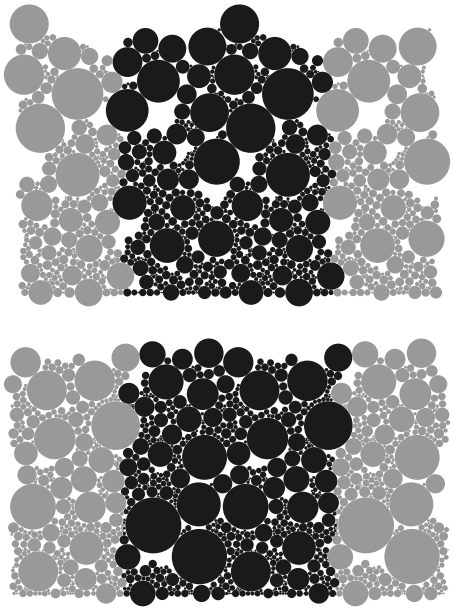

FIG. 3. Two examples of small-scale packings constructed by means of random (top) and potential-based (bottom) deposition protocols with the same particle size distribution.

Obviously, the formation of two contacts with the underlying particles in 2D does not necessarily ensure the stability of the deposited particle. Unstable configurations arise even more frequently with polydisperse particles; see Fig. 2(a). When this is the case, further relaxation is necessary to reach a locally stable position. Let us remark that local stability rules make sense only for the deposited particle in the presence of gravity. Once the packing is constructed, each particle is supported by two underlying particles and it supports one or two other particles. As a result, the equilibrium of a particle is most of the time ensured by more than two particles and it depends on both the gravity and boundary conditions. The only way to ensure force balance for each particle is to subject the sample to dynamic simulations. For a sample constructed by a deposition protocol, further dynamic relaxation occurs to reach a real mechanical equilibrium. However, a detailed analysis in the case of monodisperse packings shows that, if the constructed sample is a random close packing, the solid fraction increases only slightly due to dynamic relaxation [23].

In the potential-based approach, we determine for each particle (to be deposited) the lowest position at the free surface as a function of its diameter. This corresponds to the minimum of the potential energy $\Psi=\Sigma_{i=1}^{N_p} y(i)$, where $y(i)$ is the vertical coordinate of particle i; see Fig. 2(b). By nature, during particle deposition according to this approach, the free surface of the packing remains nearly flat and horizontal in contrast to the random approach where the free surface is rather rough; see Fig. 3. In order to avoid wall effects, periodic boundary conditions were implemented in the horizontal direction with both deposition protocols.

III. PARAMETRIC SPACE

Our packings involve two types of parameters. The particle size distribution parameters are the size span s and the shape parameters a and b (Sec. II B). The sampling parameters control the generation of discrete ensembles of particle diameters from the CVD. These include the total number of particles N_p and the number N_c of particle size classes, as well as the minimum number of particles $N_p^{\min}$ and the minimum number of particles per class $N_{p/c}^{\min}$, which control the representativity of the ensemble. We have also two layer-by-layer filling methods: random deposition and global minimum of a configurational potential energy. In this section, we focus on the influence of sampling parameters on the solid fraction ρ as the most relevant space-filling property of polydisperse packings.

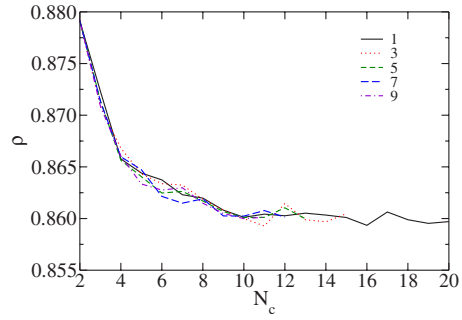

FIG. 4. (Color online) Solid fraction ρ as a function of the number N_c of particle size classes for 10^4 particles.

A. Role of sampling parameters

Obviously, if N_c and $N_{p/c}^{\min}$ are sufficiently large, ρ will be independent of sampling parameters. Conversely, we may consider a packing to be a representative volume element in terms of ρ if the latter is independent of sampling parameters. The lowest number of particles $N_p^{\min}$ required to ensure this representativity of a packing may require a huge number of particles. The limit $N_p^{\min}$ depends both on the CVD and the choice of the cutoffs $d_{\min}$ and $d_{\max}$. We may also introduce a "realizability" limit $N_p^{\max}$ on the number of particles as a function of the intended usage. For example, the number of particles in dynamic simulations, to which the generated samples can be subjected, cannot be too large (several tens of thousands). If $N_p^{\min} \leq N_p^{\max}$, the sample is both representative and realizable. Otherwise, we need to find a compromise between the sampling parameters N_c and $N_{p/c}^{\min}$ minimizing the variability of ρ with these parameters.

For a given CVD $h(d)$, the variations of ρ can be rather large as we see in Fig. 4, where the solid fraction ρ is displayed as a function of N_c for $N_p=10^4$. In this example, since N_p remains constant, the value of the minimum number of particles per class decreases with N_c but remains above $N_{p/c}^{\min}$. The size distribution parameters are $a=b=4$ and $s=0.97$, corresponding to a double-curved CVD (see Fig. 1). The solid fraction ρ declines rapidly with N_c and saturates at $N_c \simeq 10$. Hence, for this distribution, $N_c \geq 10$ ensures the representativity of the sample in ρ.

The effect of the total number of particles N_p on the solid fraction manifests itself at the extreme points of the size distribution. In the case where N^i is a decreasing (respectively, increasing) function of d^i in the range $i=1,\ldots,N_c$, the

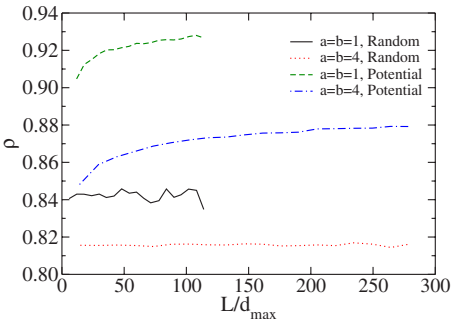

FIG. 5. (Color online) Solid fraction ρ as a function of box width L normalized by the maximum diameter $d_{\max}$ for $N_p=10$ and $s=0.97$, two different CVD and two deposition protocols.

class of the largest (respectively, smallest) particles contains $N_{p/c}^{\min}$ particles. This means that, if the extreme particles sizes are well represented, then the generated sample of particles is statistically well defined and the effect of N_p on the solid fraction is correlated with that of $N_{p/c}^{\min}$.

In the case of a nonmonotonous variation of N^i with d^i, corresponding to a double-curved CVD, both smallest and largest particles are concerned. Clearly, the representativity of the class of the largest particles can be described in terms of their number N^i as in the case of a monotonous distribution. But, the volume fraction f_v^i of smallest particles might be insufficient for a choice of $N_{p/c}^{\min}$ based on the class of the largest particles. In other words, for space-filling aptitude of the particles, the important parameter is the volume fraction f_v^i for small particles and the number of particles N^i for large particles. Most of the time, for a constant measure Δd_i (independent of i), these two conditions can be reconciled since N^i is a decreasing function of particle diameter d^i. For example, for a uniform distribution by volume fractions (where $f_v^i \propto N^i (d^i)^2$ is constant), N^i decreases as $(d^i)^{-2}$. Otherwise, the bulk representativity of small particles cannot be satisfied unless the measure Δd_i decreases with i. A geometric sequence $d_{\min}^i = d_{\min}\alpha^i$ is a possible choice. The parameter α can then be adjusted in order to ensure the representativity of largest particles in the distribution.

B. Finite-size effect

In layer-by-layer construction of a sample inside a box, the solid fraction may also be influenced by the dimensions of the box. Typically, a potential-based protocol tends to fill a layer until no more place is left, a new layer being then initiated. But it often happens that a minimum position can be found in a layer for a small particle but not for a large one. When a new layer is initiated with a large particle, the latter will partially screen the sites unfilled by small particles in the lower layer, creating thus large pores, which will no more be reached by deposited particles. The probability that this can happen decreases with the width of the box. In a wide box, smaller and larger particles can combine in many more conformations to fill a layer and the number of such conformations decreases if the width is reduced. This effect is shown in Fig. 5, where ρ is plotted as a function of box width L for $N_p=10$ and $s=0.97$, two different CVDs and two deposition protocols. With the potential-based protocol, the solid fraction increases logarithmically with L over one decade. Independently of the distribution, the rate of increase of ρ is about 0.02 per decade for the investigated range, i.e., up to 10^5 particles. In the case of random deposition, ρ is sensibly independent of L. This is consistent with the fact that during random deposition, in contrast to potential-based protocol, the choice of the deposition site of each particle is independent of its size. For the investigation of solid fraction in sections below, the width was kept around $L/d_{\max}=100$ in order to avoid this size effect.

C. Accessible domains of distribution parameters

For a systematic investigation of polydisperse packings, a high number of particles N_p is needed for the representativity of the samples generated according to a size distribution. Technically, N_p is bounded by a "realizability" limit $N_p^{\max}$ (see Sec. III A). For a given set of sampling parameters N_c and $N_{p/c}^{\min}$, a sample can be generated only if the required number of particles N_p satisfies the condition

$$N_p < N_p^{\max}. \tag{13}$$

However, at given values of sampling parameters, this condition cannot be satisfied by all combinations of distribution parameters a, b, and s. Figure 6 displays the domain of accessible values projected on the space of shape parameters a and b for two values of s and several values of $N_p^{\max}$. It is remarkable that the general aspect of the accessible domain is weakly dependent on the parameters and it expands slowly with N_p. For $N_p<10^6$, the values larger than $a=b=10$ cannot be realized. On the other hand, for strictly convex CVD ($a=1$), the limit value of b is about 4 whereas for strictly concave CVD ($b=1$) the limit value of a is about 7. The shape of the accessible domain is not symmetric about the line $a=b$. The accessible values of $a$and b are all the more reduced as the small particle classes are more populated. This restriction is more important for the points located above the line $a=b$, i.e., for $a<b$. We note that uniform distributions in diameter ($a=3$ and $b=1$) and by volume fractions ($a=b=1$) are inside the accessible domain.

D. Coefficient of uniformity

Although the extreme particle diameters $d_{\min}$ and $d_{\max}$ are well defined in a numerical approach, the sampling of smallest and largest particles in a real granular material is problematic. On one hand, the smallest sampled particles might represent a negligible volume fraction and, on the other hand, the largest sampled particles are not necessarily representative of the statistics of large particles. For this reason, s is not a well-defined experimental parameter for the span of a particle size distribution. In soil mechanics, the span is generally characterized by the "coefficient of uniformity" $C_u=d_{60}/d_{10}$, where d_x designs the diameter for which the volume fraction of smaller particles is equal to $x\%$. C_u corresponds roughly to the slope of the size distribution. It varies from 1, for a monodisperse distribution, to values above 5 for a well-graded soil [14]. From Eq. (11), we have

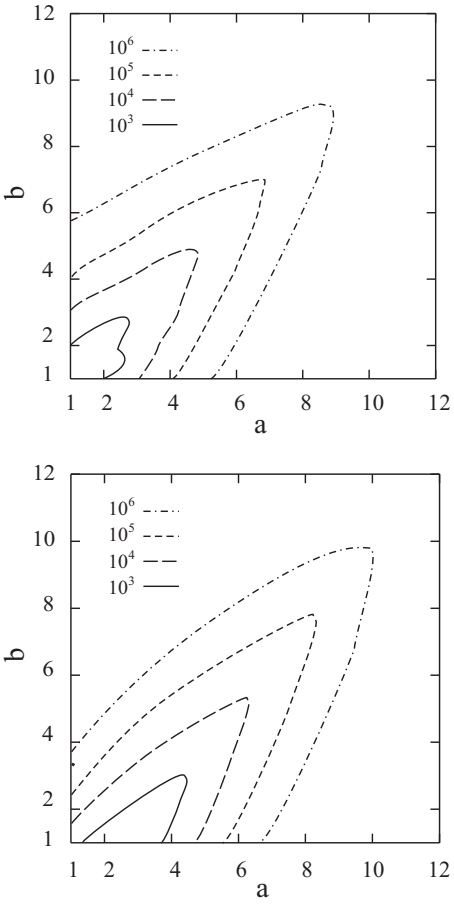

FIG. 6. Domains of statistically accessible shape parameters a and b for two different values of size span $s=0.1$ (top) and $s=0.97$ (bottom) and for several values of the maximum number of particles $N_p^{\max}$.

$$C_u = \frac{h^{-1}(0.6)}{h^{-1}(0.1)}. \tag{14}$$

It is easy to see that for our CVD, $C_u \leq 6$ for $a \geq 1$ and $b \geq 1$. Larger values of C_u can be obtained for $a<1$ or $b<1$. In view of comparison to real materials, it is interesting to evaluate the relation between C_u and s, as well as the influence of the shape parameters a and b.

Figure 7 displays C_u as a function of s for several values of shape parameters. In all cases, C_u is an increasing function of s, but at a rate which strongly depends on the shape parameters. For CVDs favoring the number of large particles ($a=3$, $b=1$; $a=4$, $b=2$), C_u increases almost linearly with s from 1 to $\simeq 2$. For CVDs favoring small particles ($a=1$, $b=3$; $a=2$, $b=4$), C_u increases nonlinearly with s and exceeds 2. For the uniform distribution by volume fractions ($a=b=1$), C_u is a highly nonlinear function of $s$and reaches its largest value 6 corresponding to $d_{60}/d_{10}=6$, as it should for a uniform distribution by volume fractions. The fact that the coefficient of uniformity increases with s indicates that it can be used to characterize the span of the distribution. But Fig. 7 underlines also the important role of the shape parameters a and b, in addition to s, in the construction of a well-graded

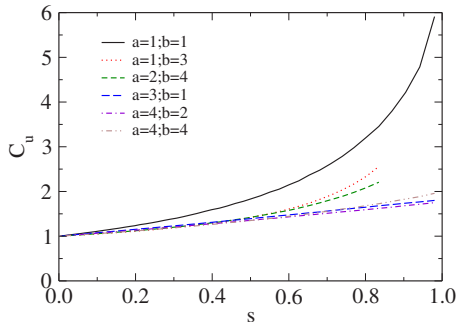

FIG. 7. (Color online) Coefficient of uniformity C_u as a function of size span s for several values of shape parameters a and b.

sample. Several isovalue plots of C_u are shown in Fig. 8 for $N_p=10^6$ and $s=0.97$. We see that a given value of C_u can be obtained for different combinations of shape parameters. The range of possible combinations is, however, strongly reduced for high values of C_u occurring in the neighborhood of $a=b=1$.

IV. SPACE-FILLING PROPERTIES

In this section, we analyze the way the particles assemble to fill the space for different size distribution parameters and our two particle deposition protocols. We consider three different space-filling properties: solid fraction ρ, radial distribution function $g(r)$, and a radial volume distribution function $\rho(r)$, which describes the correlations of solid fractions. Unless stated explicitly, all the data presented below were obtained for samples prepared with $N_c=10$, $N_{p/c}^{\min}=10$, $N_p^{\min}=3.10^4$, and $N_p^{\max}=10^5$. The span s will be varied from 0.02 to 0.97.

Each plot shown in the sections below represents about 50 data points, each point corresponding to the average of two independent depositions. The simulation of deposition of 10^5 particles by the potential-based method takes nearly 15 minutes on a Mac G5 computer. For some plots (in Figs. 7, 10, 14, 19, 21, and 22) the data points for large values of s are

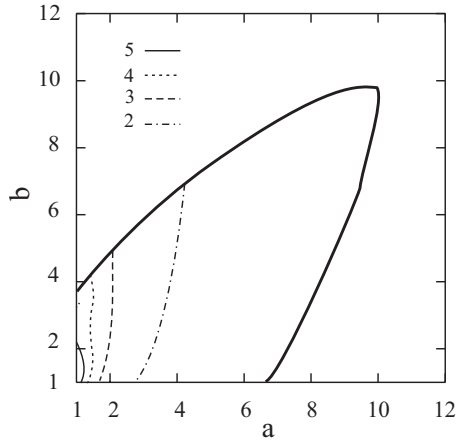

FIG. 8. Isovalue lines for several values of the coefficient of uniformity C_u for $N_p=10^6$ and $s=0.97$ inside the accessible domain marked by its contour in thick solid lines.

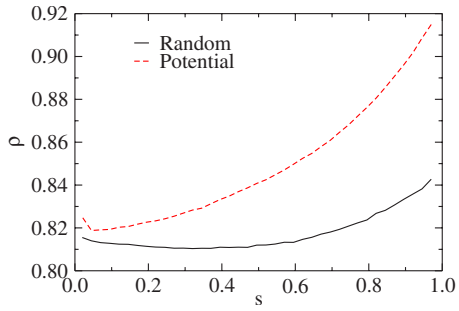

FIG. 9. (Color online) Solid fraction ρ as a function of size span s for random and potential-based deposition protcols in the case of uniform distribution by volume fractions.

not statistically accessible (for $N_p^{\max} < 10^5$) and thus these plots could not be traced for the whole range of $s \in [0.02, 0.97]$.

A. Solid fraction

The solid fraction ρ is shown in Fig. 9 as a function of size span s for random and potential-based methods in the case of uniform distribution by volume fractions. As expected, the potential-based method yields considerably higher levels of solid fraction as s increases. This suggests that the polydisperse packings are thus more sensitive to the preparation protocol. For both methods, ρ first decreases with s, passes by a minimum, and then increases to much higher values. The lowest values of ρ are $\simeq 0.82$ for the potential-based method and $\simeq 0.81$ for the random method. These values correspond to the order of magnitude of the solid fraction in a quasimonodisperse random close packing. The highest values are $\simeq 0.91$ for the potential-based method and $\simeq 0.84$ for the random method.

We observe similar trends for all values of shape parameters a and b. This is shown in Fig. 10 for the potential-based method. The solid fraction declines in the range $s < 0.1$. Then, it increases slowly with s in the range $0.1 < s < 0.4$. In this range, the values of ρ are sensibly the same independently of shape parameters except for $a=b=1$. Beyond $s \simeq 0.4$, ρ increases faster for distributions favoring the number of small particles ($a=1$, $b=3$; $a=2$, $b=4$) than those favoring the number of large particles ($a=3$, $b=1$; $a=4$, $b=2$). For each value of s, the solid fraction ρ for the uniform distribution by volume fractions ($a=b=1$) is higher than those for all other values of shape parameters.

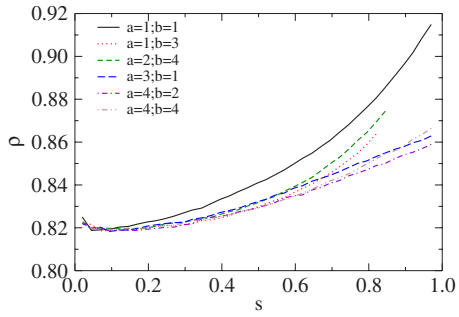

FIG. 10. (Color online) Solid fraction ρ as a function of size span s in the case of the potential-based deposition protocol for several values of shape parameters a and b.

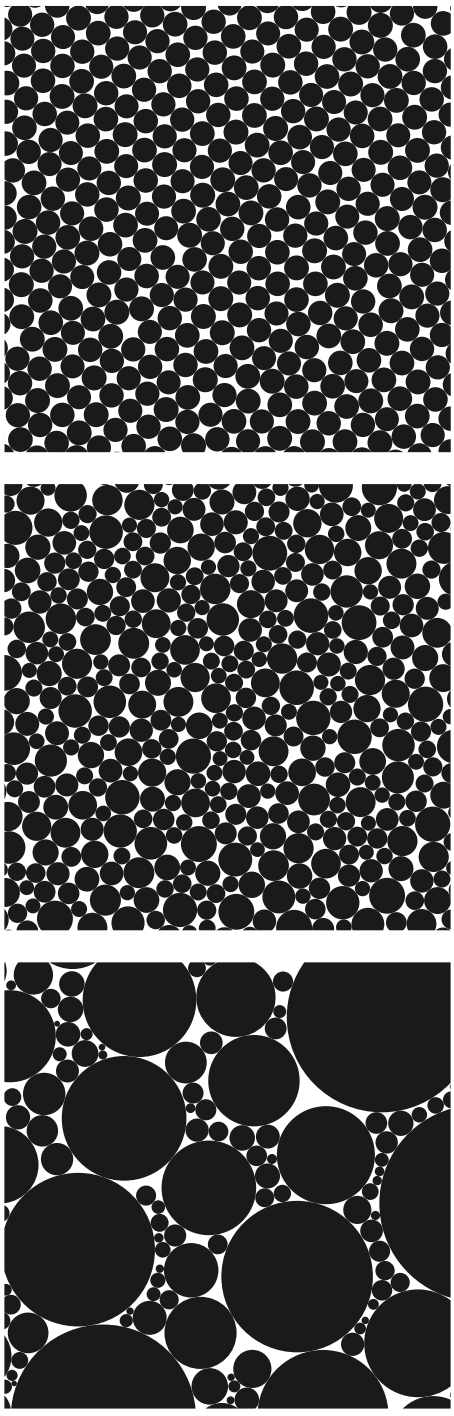

FIG. 11. Snapshots of samples for $s=0.02$ (top), $s=0.42$ (middle), and $s=0.97$ (bottom).

Figure 11 shows snapshots of the samples for three different values of s generated for $a=b=1$. At very low values of s ($s<0.1$), the arrangement is quasimonodisperse involving long-range order and dislocations. The coordination number is about 4. The larger values of ρ ($\rho > 0.82$) in this range are due to local triangular structures inside a globally square lattice of particles. The decrease of ρ with s in this range

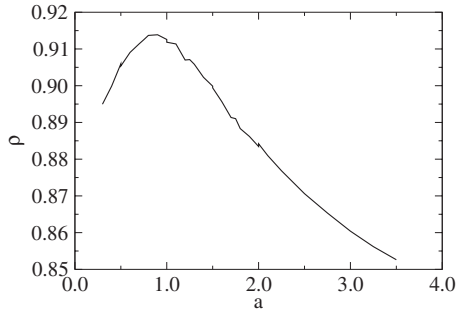

FIG. 12. Solid fraction ρ as a function of shape parameter a for $b=1$ and $s=0.97$.

corresponds to the well-known order-disorder transition observed in 2D monodisperse granular media due to the perturbation of an initially triangular lattice in the presence of a small amount of polydispersity [13]. At larger values of s $(0.1<s<0.4)$, we observe a weakly polydisperse arrangement involving only local (short-range) order. The solid fraction increases slowly with s although for $s<0.4$ the smallest particles are not yet large enough to fit into the pores between the largest particles. This condition occurs precisely at $s=0.4$ for a square lattice. The faster increase of ρ with s beyond $s\simeq 0.4$ is thus a consequence of an increasingly higher number of pore-filling small particles.

Figure 12 shows the solid fraction as a function of a for $s=0.97$ and $b=1$. We see that the largest value of solid fraction occurs for $a=1$. We checked that this is also true for all values of s, with a decreasing maximum solid fraction when s decreases. Remark that with $b=1$, the CVD of particle diameters is reduced to a power law

$$h(d) = d^a, \tag{15}$$

or equivalently, the probability density function of particle diameters is

$$N(d) = (\alpha + 1)d^{-\alpha}, \tag{16}$$

with $\alpha=3-a$. The maximum solid fraction is thus obtained for $\alpha\simeq 2$. It is interesting to notice that this value of the exponent for the optimal space filling was obtained also for packings constructed by very different filling protocols [11].

In fact, two conditions are required to fill efficiently the pores: (1) a broad size distribution, which corresponds to higher values of s ($s>0.4$ in our simulations), and (2) a large number of smaller particles, controlled in our model by the shape parameters a and b. The broad size distributions favoring smaller particles lead thus to enhanced levels of solid fraction. According to Fig. 10, these conditions appear to be optimally fulfilled for uniform distribution by volume fractions and with the potential-based method. In other words, equal volume fractions provide the best match between the volumes of particles and pores.

B. Radial distribution function

The spatial order in polydisperse packings can be evaluated by means of the radial distribution function $g(r)$ of the radial positions r of particle centers, defined by

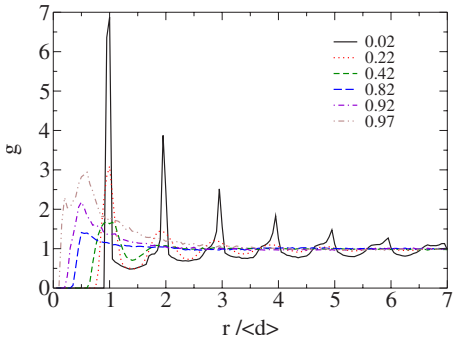

FIG. 13. (Color online) Radial distribution function g as a function of radial distance r normalized by the average particle diameter $\langle d\rangle$ for uniform size distribution by volume fractions and different values of size span s.

$$g(r) = \frac{n(r)}{n}, \tag{17}$$

where $n(r)$ is the average number density of particle centers at a distance r from the given particle and n is the average number density of the packing. The variations of g as a function of r reflect thus the average placement of the surrounding particles. Figure 13 shows $g(r)$ for uniform size distribution by volume fractions and different values of s. For $s<0.4$, we observe the signature of short-range order with regular peaks of decreasing amplitude at positions which are multiples of the average diameter $\langle d\rangle$. The correlation length of several average particle diameters, and the amplitudes, decrease as s increases. For $s>0.4$, only the first peak survives and shifts to values below the average diameter with an increasing amplitude. Hence, the size span $s=0.4$ corresponds also to transition from short-range order to practically no correlation beyond the first "shell" around the particles.

The observed shift of the peaks in Fig. 13 towards positions below the average diameter indicates that for polydisperse granular materials we should distinguish two different length scales: (1) the average diameter $\langle d\rangle$, and (2) the mean distance ℓ between particle centers. Figure 14 shows $\ell/\langle d\rangle$ as a function of s for several values of shape parameters. In weakly polydisperse packings $(s<0.2)$, we have $\ell\simeq\langle d\rangle$. Then, the ratio $\ell/\langle d\rangle$ increases with s all the more the shape

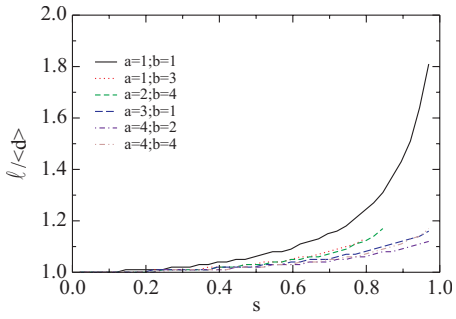

FIG. 14. (Color online) Ratio of the mean distance between particle centers ℓ to the average particle diameter $\langle d\rangle$ as a function of size span s for several values of shape parameters a and b.

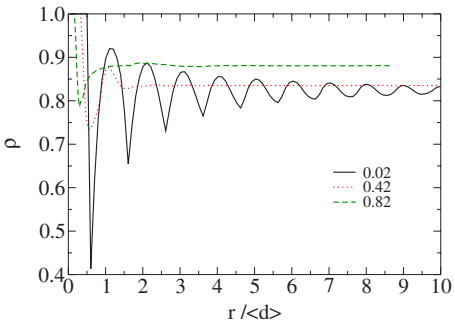

FIG. 15. (Color online) Average solid fraction ρ as a function of radial distance r from a given particle center normalized by the average diameter $\langle d \rangle$ for uniform distribution by volume fractions and three values of size span s.

parameters favor small particles. The trends observed in Fig. 14 are comparable with those observed previously for C_u as a function of s in Fig. 7. Larger values of C_u lead to higher values of the ratio $\ell/\langle d \rangle$ and solid fraction.

We may also legitimately ask whether the radial distribution function is the best representation of pair correlations in polydisperse granular media. The number density $n(r)$ is a natural quantity for molecular systems or monodisperse granular media where the constituents have all nearly the same volume. In polydisperse granular media, we need to account for particle volumes. It seems thus pertinent to consider the solid fraction $\rho(r)$ as a function of radial positions r of the particles. In practice, the solid fraction $\rho(r)$ can be calculated inside circular shells of increasing radius r centered on particle centers. Figure 15 shows $\rho(r)$ for uniform distribution by volume fractions for three values of size span s. In all cases, $\rho(r)$ is equal to 1 for $r \leq d_{\min}/2$ and tends to the packing solid fraction ρ at large values of r. As in the radial distribution function, the solid fraction oscillates between peaks and valleys of decreasing amplitude with a period of nearly $\langle d \rangle$ at low values of s. At larger polydispersities, one mainly observes a marked valley following the initial plateau and a nearly constant increase towards ρ. This valley represents the void space between a particle and its first neighbors. In the pore-filling regime ($s > 0.4$), the material can be considered as homogeneous beyond almost two average diameters. It should be, however, borne in mind that the average diameter in this regime corresponds to many small particle diameters $d_{\min}$. As s increases, the correlation length decreases slightly in units of the average particle diameter.

V. CONTACT NETWORK

The solid fraction and radial distribution function account for the metric disorder depending on particle size distributions. However, most mechanical properties of granular media, such as force transmission and dilatancy, result from the topological disorder of the contact network. In this section, we study the influence of size distribution on the connectivity and anisotropy of the contact network.

A. Connectivity

Monodisperse particles can, in principal, assemble to form triangular packings with coordination number $z=6$.

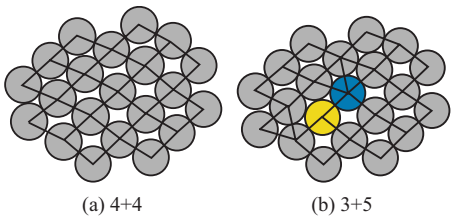

FIG. 16. (Color online) Illustration of two particles of 4 contacts (4+4) transforming to two particles of 3 (yellow) and 5 (blue) contacts, respectively, due to a small difference in size distribution.

However, this upper limit can never be reached without fine adjustment of particle positions due to geometrical mismatches related to steric exclusions and numerical precision. In the presence of the slightest perturbation of the assembly, the coordination number collapses to $z=4$. For example, at weak polydispersity ($s=0.02$), for a sample prepared by the potential-based protocol, we get $z=4$. To explain this, a common argument is that each deposited particle is supported by two particles and it supports two other particles. This argument implies that *each* particle should have exactly 4 contact neighbors. But, this is not what we observe. For $s=0.02$, only a proportion $\simeq 0.8$ of particles have 4 contacts. Other particles have either 3 or 5 contacts at equal proportions $\simeq 0.1$. It is easy to see that this configuration again leads to an *average* coordination number of 4.

The point is that, during particle deposition, each particle is, by construction, supported by two particles, but it does not necessarily support two other particles. Figure 16 shows an example where two particles each with 4 contacts transform to two particles with 3 and 5 contacts, respectively, due simply to the disposition of an intermediate particle to form a contact with one or the other. This transformation from 4+4 configuration to 3+5 configuration conserves the average coordination number. Hence, the particle size distribution manifests itself mainly through the variability of local coordination numbers. Figure 17 displays a snapshot of a sample for $s=0.22$ where the particles of 3 and 5 contacts are marked. We indeed observe that these particles occur mostly in pairs and in zones of strong disorder correlated over long distances in space.

In order to characterize the variations of local coordination numbers, we consider here the "connectivity function" P_k defined as the proportion of particles inside a sample with exactly k contacts. We have $\Sigma_k P_k = 1$ and $\Sigma_k k P_k = z$. Figure 18 shows the plots of P_k for different values of k as a function of size span s for uniform distribution by volume fractions. As stated above, at very narrow spans we have $P_4 \simeq 0.8$ and $P_3 = P_5 \simeq 0.1$. As s increases, P_3 and P_5 increase together at the expense of P_4, which declines to 0.6 at $s=0.2$. In the range $s < 0.2$, $P_k = 0$ for all$k$ except $k=3$, 4, and 5. The evolution of topological disorder in this range is thus governed by the growth of two populations of particles with 3 and 5 contacts.

The populations of particles with 6 and 2 contacts appear at $s=0.2$ and increase with s. At the same time, P_5 stops growing and begins to decline beyond $s \simeq 0.4$. P_4 continues to decline as new populations appear whereas P_2 keeps increasing all the way. All other populations first begin to grow

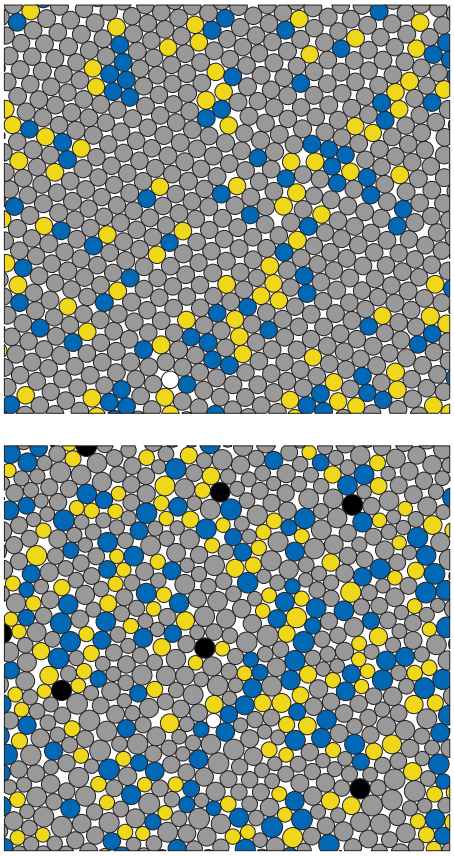

FIG. 17. (Color online) Snapshots of samples for $s=0.02$ (top) and $s=0.2$ (bottom) marked according to the local coordination number of the particles: 2 contacts in white, 3 contacts in yellow (light gray), 4 contacts in intermediate gray, 5 contacts in blue (dark gray), and 6 contacts in black.

up to a certain level and then decline asymptotically to a value characterizing a very polydisperse packing. The trends are sensibly similar for other values of shape parameters (not shown here). It should be noted that particles with many more contacts (up to $k=50$) appear in the samples at high levels of s but they are marginal compared to the populations already shown in Fig. 17.

The particles with 2 contacts are the small particles which are supported by two particles but which support none. Hence, P_2 represents the importance of geometrical arching

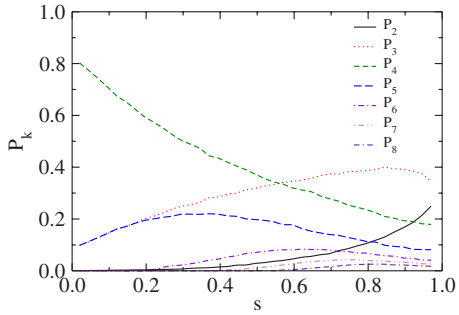

FIG. 18. (Color online) The connectivity functions P_k for different values of k as a function of size span s for uniform distribution by volume fractions.

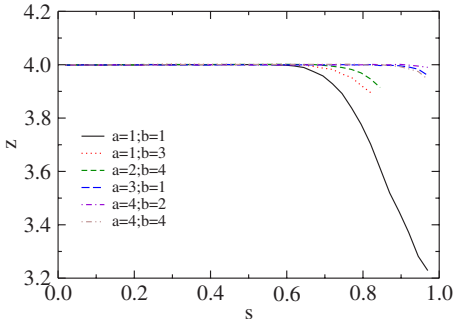

FIG. 19. (Color online) Coordination number z as a function of size span s for several values of distribution shape parameters a and b.

which leads to the screening of smallest particles. This population grows rapidly with polydispersity and does not seem to saturate at highest values of s. A consequence of the growth of this population is to reduce the coordination number below 4; see Fig. 19.

B. Fabric anisotropy

The anisotropy of the contact network is known as a major mechanism of shear strength in granular media [32–34]. This anisotropy can be expressed through the probability density function $P(\theta)$ of the orientations θ of normals $\boldsymbol{n}$ to the contact planes. Figure 20 displays $P(\theta)$ for uniform distribution by volume fractions for several values of s. This is a bimodal symmetric distribution with two peaks at $\theta=45^\circ$ and $\theta=135^\circ$ for low values of s. The peaks flatten with s and tend to the center of the distribution at $\theta=90^\circ$. Angular distributions of bimodal feature have also been observed in experiments and dynamic simulations of granular beds prepared by random deposition [35].

The anisotropy of $P(\theta)$ can be extracted from the fabric tensor F_{ij} defined by [32]

$$F_{ij} = \int_0^\pi n_i(\theta) n_j(\theta) P(\theta) d\theta. \tag{18}$$

The first order anisotropy of the distribution $P(\theta)$ is given by

$$a_c = 2(F_1 - F_2), \tag{19}$$

where F_1 and F_2 are the principal values of F_{ij}. However, this definition applied to the distributions observed in Fig. 20 yields low values of a_c as a result of the symmetry of these

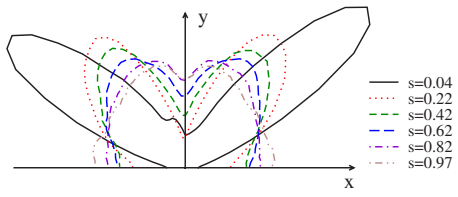

FIG. 20. (Color online) Polar representation of the probability density function $P(\theta)$ of the orientations θ of contact normals for uniform distribution by volume fractions and several values of particle size span s.

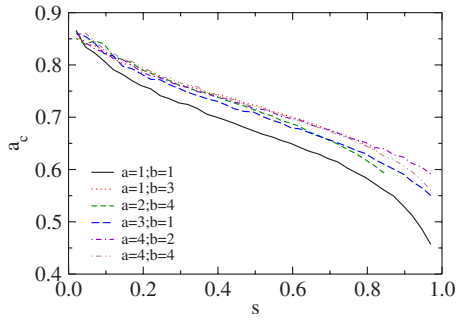

FIG. 21. (Color online) Fabric anisotropy a_c over a quarter as a function of size span s for several values of shape parameters a and b.

distributions. It is thus reasonable to restrict the definition of the fabric tensor in Eq. (18) to the subinterval $[0,\pi/2]$. The corresponding anisotropy a_c then represents the importance of the peak in each subinterval. Figure 21 shows this half-interval anisotropy as a function of s for several values of shape parameters. We see that a_c falls off with s from 0.85 for $s \simeq 0$ to values below 0.5 for $s \simeq 1$ in the case of uniform distribution by volume fractions. This behavior does not depend crucially on the shape parameters, the lowest anisotropies being observed for $a=b=1$. We also remark that, the rate of variation of a_c with $s$involves two transitions occurring at $s \simeq 0.2$ and $s \simeq 0.8$.

The bond-orientational order of the packing can also be characterized in terms of the scalar order parameters ψ_k defined as [36]

$$\psi_k = |\langle e^{ki\theta_c} \rangle_c|, \tag{20}$$

where $i^2=-1$ and the average is taken over all contact directions θ_c in the packing. The value of k sets the symmetry of the reference configuration. For example, ψ_6 measures how close the configuration is to a perfect sixfold symmetry: ψ_6 varies from 0 in a random isotropic arrangement to 1 in a perfect hexagonal particle arrangement. In our packings, the reference configuration is a monodisperse packing of mean coordination number $z=4$ (Fig. 18, top).

The query is how this fourfold symmetry changes with size span s. Figure 22 shows ψ_4 as a function of s for different values of shape parameters. For uniform distribution by

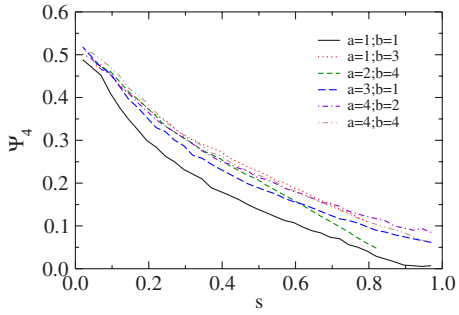

FIG. 22. (Color online) Fourfold bond-orientational order parameter ψ_4 as a function of size span s for several values of shape parameters a and b.

volume fractions, ψ_4 declines from $\simeq 0.5$ in the case of a nearly monodisperse arrangement down to 0 at $s \simeq 1$. For other values of shapes parameters, ψ_4 decreases more slowly towards a weak residual order. The behavior of ψ_4 as a function of s is comparable to that of the anisotropy a_c as calculated over the half-interval $[0,\pi/2]$. This means that, since z is always equal or close to 4, the value of ψ_4 is directly linked with the fabric anisotropy as defined by Eq. (19). We checked that ψ_6 in our samples is nonzero butremains weak compared to ψ_4.

VI. CONCLUSION

In this paper, a methodology was developed for a systematic investigation of microstructure in densely packed polydisperse granular media. We took care of the details of sampling procedure and filling protocol allowing us to generate dense collections of circular particles with a prescribed cumulate volume distribution and constrained by explicit criteria of statistical representativity. A model of cumulate volume distributions of the particles, based on β distribution, was proposed. This model accounts both for size span (or the width) and the shape of size distributions. These cumulate volume distributions can be simple- or double-curved, and well-known size distributions such as monodisperse, bidisperse, and power laws are particular instances of this function.

It was shown that statistically well-represented ensembles of particle diameters could be obtained only for a portion of the parameter space when the total number of data (particle diameters) is bounded. This provides an interesting and quantitative basis for the practically accessible particles size distributions in polydisperse granular media. We then addressed in this framework two major aspects of polydisperse media: (1) space-filling properties in terms of solid fraction and radial distribution functions and (2) contact network in terms of connectivity disorder and anisotropy. It turns out that highly polydisperse media are more sensitive to the filling method as it was shown by comparing two different deposition methods. The solid fraction increases in a strongly nonlinear manner with size span and a transition occurs from a basically "topological disorder" regime to a "metric disorder" regime around a particular value of size span depending on shape parameters.

In the first regime, the particle size distribution manifests itself mainly through the variability of local coordination numbers. The overall connectivity of the contact network is dominated by the population of particles with four contacts, but a continued bifurcation to particles with three and five contacts is observed as the size span increases. In this regime, short-range correlations of particle positions prevail, and the solid fraction evolves slowly with size span.

The metric disorder regime is governed by the aptitude of the small particles to fill the pores left by larger particles. The connectivity is broadly distributed and a large population of particles with two contacts is present. The positions of neighboring particles are no more correlated, the only local order being the presence of a low-density region around each particle. We find that the solid fraction increases con-

siderably with size span in this regime and the highest values of solid fraction are obtained with the uniform distribution by volume fractions. This is obviously a consequence of an increasingly higher number of pore-filling small particles and suggests that equal volume fractions provide the best match between the volumes of particles and pores. In the highly polydisperse limit, the material is homogeneous beyond only about two average particle diameters, corresponding to a vast population of small particles. A well-known example of packings in this limit is the case of random appollonian packings often associated with scale invariance and power-law distributions of particle diameters [11,16].

The orientational ordering of the contact network was investigated by means of the fabric anisotropy and a scalar order parameter. The contact orientations define a bimodal distribution induced by the deposition protocol. The concentration of contact normals in each mode can be characterized by a fabric anisotropy. We showed that the fourfold orientational order is linked with the fabric anisotropy in each mode and it decreases with size span. In particular, the uniform distribution by volume fractions is practically isotropic at high degrees of polydispersity.

This work will be pursued in several directions. In the first place, we would like to subject our samples to isotropic compaction and shear deformations. Various static properties such as force transmission and shear strength can be investigated as a function of size distribution parameters. The origins of shear strength in highly polydisperse granular media is an open issue with potential applicability to soils and powder blends. It seems *a priori* not clear how shear strength will increase with size span. In fact, the reduction of anisotropy with size span is rather consistent with a decrease of shear strength. Another promising direction of research concerns the 3D extension of this investigation. This extension is possible due to numerical efficiency of purely geometrical calculations involved in this approach. It is also of paramount importance to verify our findings in a 3D configuration. For example, it would be interesting to examine the uniform distribution by volume fractions in order to see whether they provide most compact samples also in three dimensions. In the same way, the effect of polydispersity in the "pore-filling" regime might turn out to be different since the pores in three dimensions percolate throughout the space.

[1] J. Duran, S. Luding, E. Clement, and J. Rajchenbach, J. Mol. Liq. **76**, 221 (1998).
[2] K. Ceylan and G. Kelbaliyev, Powder Technol. **119**, 173 (2001).
[3] P. Acker, *Statistical Models for Fracture in Disordered Media* (North Holland, Amsterdam, 1990), Chap. 3.2, pp. 52–58.
[4] F. de Larrard and T. Sedran, Cem. Concr. Res. **32**, 1699 (2002).
[5] T. Aste and D. Weaire, *The Pursuit of Perfect Packing* (Institute of Physics Publishing, Bristol, 2000).
[6] S. Assouline and Y. Rouault, Colloids Surf., A **127**, 201 (1997).
[7] P. F. Luckham and M. A. Ukeje, J. Colloid Interface Sci. **220**, 347 (1999).
[8] M. Semmler, J. Ricka, and M. Borkovec, Colloids Surf., A **165**, 79 (2000).
[9] A. de Leon, O. Pizio, and S. Sokolowski, J. Colloid Interface Sci. **298**, 306 (2006).
[10] H. J. Herrmann, R. Mahmoodi Baram, and M. Wackenhut, Physica A **330**, 77 (2003).
[11] T. Aste, Phys. Rev. E **53**, 2571 (1996).
[12] M. Ammi, D. Bideau, and J. P. Troadec, J. Phys. D **20**, 424 (1987).
[13] A. Gervois and D. Bideau, in *Disorder and Granular Media*, edited by D. Bideau (Elsevier, Amsterdam, 1993).
[14] J. K. Mitchell and K. Soga, *Fundamentals of Soil Behavior*, 3rd ed. (Wiley, New York, 2005).
[15] M. Wackenhut, S. McNamara, and H. Herrmann, Eur. Phys. J. E **17**, 237 (2005).
[16] P. S. Dodds and J. S. Weitz, Phys. Rev. E **65**, 056108 (2002).
[17] M. Renouf and P. Alart, Comput. Methods Appl. Mech. Eng. **194**, 2019 (2005).
[18] M. Renouf, F. Dubois, and P. Alart, J. Comput. Appl. Math. **168**, 375 (2004).
[19] R. Jullien and P. Meakin, Colloids Surf., A **165**, 405 (2000).
[20] M. J. Vold, J. Colloid Sci. **14**, 168 (1959).
[21] W. M. Visscher and M. Bolsterli, Nature (London) **239**, 504 (1972).
[22] T. I. Quickenden and G. K. Tan, J. Colloid Interface Sci. **48**, 382 (1974).
[23] I. Bratberg, F. Radjai, and A. Hansen, Phys. Rev. E **66**, 031303 (2002).
[24] A. Taboada, K. J. Chang, F. Radjai, and F. Bouchette, J. Geophys. Res. **110**, 1 (2005).
[25] M. P. Allen and D. J. Tildesley, *Computer Simulation of Liquids* (Oxford University Press, Oxford, 1987).
[26] H.-G. Matuttis, S. Luding, and H. J. Herrmann, Powder Technol. (to be published).
[27] J. Moreau, Eur. J. Mech. A/Solids **supp.**, 93 (1994), formulation mathematiques tire du livre Contacts mechanics.
[28] M. Jean, Comput. Methods Appl. Mech. Eng. **177**, 235 (1999).
[29] F. Radjai, Comput. Phys. Commun. **121-122**, 294 (1999).
[30] R. Jullien, P. Jund, D. Caprion, and D. Quitmann, Phys. Rev. E **54**, 6035 (1996).
[31] R. Jullien, P. Meakin, and A. Pavlovitch, J. Phys. A **25**, 4103 (1992).
[32] M. Satake, in *Proceedings of the IUTAM Symposium on Deformation and Failure of Granular Materials, Delft*, edited by P. A. Vermeer and H. J. Luger (A. A. Balkema, Amsterdam, 1982), pp. 63–68.
[33] L. Rothenburg and R. J. Bathurst, Geotechnique **39**, 601 (1989).
[34] F. Radjai, D. E. Wolf, M. Jean, and J.-J. Moreau, Phys. Rev. Lett. **80**, 61 (1998).
[35] F. Calvetti, G. Combe, and J. Lanier, Mech. Cohesive-Frict. Mater. **2**, 121 (1997).
[36] A. R. Kansal and T. M. T. S. Torquato, J. Chem. Phys. **113**, 4844 (2000).